Atmos. Chem. Phys., 22, 2079–2093, 2022
https://doi.org/10.5194/acp-22-2079-2022

Atmospheric Chemistry and Physics
Open Access
EGU

From the middle stratosphere to the surface, using nitrous oxide to constrain the stratosphere–troposphere exchange of ozone

Daniel J. Ruiz and Michael J. Prather

Department of Earth System Science, University of California Irvine, Irvine, CA 92697-3100, USA

Correspondence: Daniel J. Ruiz (djruiz@uci.edu)

Received: 29 July 2021 – Discussion started: 6 August 2021
Revised: 7 December 2021 – Accepted: 7 December 2021 – Published: 15 February 2022

Abstract. Stratosphere–troposphere exchange (STE) is an important source of tropospheric ozone, affecting all of atmospheric chemistry, climate, and air quality. The study of impacts needs STE fluxes to be resolved by latitude and month, and for this, we rely on global chemistry models, whose results diverge greatly. Overall, we lack guidance from model–measurement metrics that inform us about processes and patterns related to the STE flux of ozone (O_3). In this work, we use modeled tracers (N_2O and $CFCl_3$), whose distributions and budgets can be constrained by satellite and surface observations, allowing us to follow stratospheric signals across the tropopause. The satellite-derived photochemical loss of N_2O on annual and quasi-biennial cycles can be matched by the models. The STE flux of N_2O-depleted air in our chemistry transport model drives surface variability that closely matches observed fluctuations on both annual and quasi-biennial cycles, confirming the modeled flux. The observed tracer correlations between N_2O and O_3 in the lowermost stratosphere provide a hemispheric scaling of the N_2O STE flux to that of O_3. For N_2O and $CFCl_3$, we model greater southern hemispheric STE fluxes, a result supported by some metrics, but counter to the prevailing theory of wave-driven stratospheric circulation. The STE flux of O_3, however, is predominantly northern hemispheric, but evidence shows that this is caused by the Antarctic ozone hole reducing southern hemispheric O_3 STE by 14 %. Our best estimate of the current STE O_3 flux based on a range of constraints is $400\,\mathrm{Tg(O_3)\,yr^{-1}}$, with a 1σ uncertainty of ± 15 % and with a NH : SH ratio ranging from 50 : 50 to 60 : 40. We identify a range of observational metrics that can better constrain the modeled STE O_3 flux in future assessments.

1 Introduction and background

The influx of stratospheric ozone (O_3) into the troposphere affects its distribution, variability, lifetime, and, thus, its role in driving climate change and surface air pollution (Zeng et al., 2010; Hess et al., 2015; Williams et al., 2019). The net stratosphere-to-troposphere exchange (STE) flux of O_3 has a regular seasonal cycle in each hemisphere that is an important part of the tropospheric O_3 budget (Stohl et al., 2003). Such fluxes are not directly observable, and we rely on observational estimates using trace gas ratios, in particular the $O_3 : N_2O$ ratio in the lower stratosphere (Murphy and Fahey, 1994; McLinden et al., 2000), or dynamical calculations using measured/modeled winds and O_3 abundances (Gettelman et al., 1997; Olsen et al., 2004; Yang et al., 2016). The uncertainty in these estimates does not effectively constrain the wide range found in the models being used to project future ozone (Young et al., 2013, 2018; Griffiths et al., 2021). Here we present the case for using the observed variations in nitrous oxide (N_2O) from the middle stratosphere to the surface in order to constrain the STE flux of O_3. A similar case has been made for the radionuclide ^{7}Be (Liu et al., 2016), but N_2O has a wealth of model–observation metrics on hemispheric, seasonal, and interannual scales that constrain its STE flux very well (Prather et al., 2015; Ruiz et al., 2021).

Ozone-rich stratospheric air has been photochemically aged and is depleted in trace gases such as N_2O and chlorofluorocarbons (CFCs). For these trace gases, the overall cir-

culation from tropospheric sources to stratospheric destruction and back is part of the lifecycle that maintains their global abundance (Holton, 1990). For N_2O and CFCs, this cycle of (i) loss in the middle to upper stratosphere, (ii) transport to the lowermost stratosphere (Holton et al., 1995), and then (iii) influx into the troposphere produces surface variations not related to surface emissions (Hamilton and Fan, 2000; Nevison et al., 2004; Hirsch et al., 2006; Montzka et al., 2018; Ray et al., 2020; Ruiz et al., 2021). In this work, we relate our modeled STE fluxes to variations at the surface and throughout the stratosphere, linking the fluxes of N_2O to O_3 through stratospheric measurements. Our goal is to develop a set of model metrics founded on observations that are related to the STE O_3 flux and can be used with an ensemble of models to determine a better, constrained estimate for the flux, including seasonal, interannual, and hemispheric patterns. This approach is similar to efforts involving the ozone depletion recovery time (Strahan et al., 2011) and projections of future warming (Liang et al., 2020; Tokarska et al., 2020).

In a previous work (Ruiz et al., 2021; hereafter R2021), we showed that historical simulations with three chemistry transport models (CTMs) were able to match the interannual surface variations observed in N_2O. These were clearly driven by the stratospheric quasi-biennial oscillation (QBO), which appears to be the major interannual signal in stratospheric circulation and STE (Kinnersley and Tung, 1999; Baldwin et al., 2001; Olsen et al., 2019). In this work, we calculate the monthly latitudinal STE fluxes of O_3, N_2O, and $CFCl_3$ (F11), establish a coherent picture relating fluxes to observed abundances, and summarize the methods in Sect. 2. In Sect. 3, we examine the annual and interannual cycles, as well as geographic patterns, of modeled STE flux. In Sect. 4, we relate the surface variability in N_2O to its STE flux. We find some evidence to support our model result that the STE flux of depleted N_2O air is greater in the Southern Hemisphere than in the Northern Hemisphere, thus altering the asymmetry in surface emissions in the source inversions (Nevison et al., 2007; Thompson et al., 2014). In Sect. 5, we examine the lowermost stratosphere to understand the large north–south asymmetry found in O_3 STE versus N_2O or F11 STE and find a clear signal of the Antarctic ozone hole in STE. In Sect. 6, we examine the consistency of the model calculations of STE flux and derive a best estimate for the O_3 flux from this and previous studies. We summarize a sequence of model metrics, primarily using O_3 and N_2O, that can narrow the range in the tropospheric O_3 budget terms for the multi-model intercomparison projects used in tropospheric chemistry and climate assessments.

2 Methods

The modeled STE fluxes here are calculated with the UCI (University of California Irvine) CTM driven by 3 h forecast fields from the European Centre for Medium-Range Weather Forecasts (ECMWF) Integrated Forecasting System (IFS; cycle 38r1; T159L60) for the years 1990–2017, as are the calculations in R2021. The CTM uses the IFS native 160×320 Gauss grid ($\sim 1.1°$) with 60 layers, about 35 of which are in the troposphere. The stratospheric chemistry uses the linearized ozone model Linoz v3 and includes O_3, N_2O, NO_y, CH_4, and F11 as transported trace gases (Hsu and Prather, 2010; Prather et al., 2015; Ruiz et al., 2021). There is no tropospheric chemistry but rather a boundary layer e-fold to a specified abundance or a surface boundary reset to an abundance. Equivalent effective stratospheric chlorine levels are high enough to drive an Antarctic ozone hole, which is observed throughout this period. Thus, the ozone hole chemistry in Linoz v3 is activated for all years, and the amount of O_3 depleted depends on the Antarctic meteorology of that year (Hsu and Prather, 2010).

The STE flux is calculated using the e90 definition of tropospheric grid cells (Prather et al., 2011) and the change in tropospheric tracer mass from before to after each tracer transport step, as developed at UCI (Hsu et al., 2005; Hsu and Prather, 2009; Hsu and Prather, 2014). This method is precise and geographically accurate for O_3 and is self-consistent with a CTM's tracer–transport calculation (Tang et al., 2013; Hsu and Prather, 2014). Extensive comparisons with other methods of calculating STE are shown in Hsu and Prather (2014). Annual mean STE fluxes are calculated from the full 28-year (336 month) time series as 12-month running means, and the annual cycle of monthly fluxes is the average of the 28 values for each month.

R2021 modeled the surface signal of stratospheric loss with the decaying tracers, N2OX and F11X (e.g., Hamilton and Fan, 2000; Hirsch et al., 2006). These X tracers have identical stratospheric chemical loss frequencies to N_2O and $CFCl_3$, respectively, but have no surface sources and are, therefore, affected only by the stratospheric sink and atmospheric transport. The multi-decade (F11X) to century (N2OX) decays are easily rescaled using a 12-month smoothing filter to give stationary results and a tropospheric mean abundance of 320 ppb (parts per billion). We treat F11X like N2OX with the same initial conditions and molecular weight. Budgets for N2OX are reported, as in N_2O studies (Tian et al., 2020), as the teragram (hereafter Tg) of N as N_2O. These rescaled N2OX and F11X tracers are designated simply as N2O (not N_2O) and F11. Our F11 STE fluxes are, thus, unrealistically large compared to current $CFCl_3$ fluxes but can be easily compared with our N2O results.

When trying to calculate the STE flux of N_2O-depleted air across the tropopause, we found that the Hsu method was numerically noisy because the gradient across the tropopause, unlike that of O_3, was negligible. Thus, for this work, we created the complementary tracers cN2OX and cF11X; for each kilogram of the X tracer (i.e., N2OX) destroyed by photochemistry, 1 kg of its complementary tracer (cN2OX) is created. Air parcels that are depleted in N2OX (F11X) are therefore rich in cN2OX (cF11X). After crossing the

tropopause, cN2OX and cF11X are removed through rapid uptake in the boundary layer, thus creating sharp gradients at the tropopause in parallel with that of O_3. As a check, we compared the boundary layer sinks of the *c* tracers with their e90-derived STE fluxes and find that their sums are identical. The *c* tracers and their STE fluxes are rescaled, as are the X tracers, to give them a stationary time series corresponding to a tropospheric abundance of 320 ppb for their parallel X tracers. We designate these scaled tracers simply as cN2O and cF11.

3 Modeled STE fluxes

3.1 Global and hemispheric means

The 28-year mean of global O_3 STE is $390 \pm 16\,\mathrm{Tg\,yr^{-1}}$ (positive flux means stratosphere to troposphere; the $\pm$ (plus or minus) values are the standard deviation of the 28 annual means and do not represent uncertainty). This value is well within the uncertainty in the observation-based estimates (Murphy and Fahey, 1994; Olsen et al., 2001) and far from the extreme ranges of the 34 models in the latest Tropospheric Ozone Assessment Report (TOAR; Young et al., 2018), which is 150 to $940\,\mathrm{Tg\,yr^{-1}}$. The global STE flux of cN2O is $11.5 \pm 0.7\,\mathrm{Tg\,yr^{-1}}$, and that of cF11 is $23.5 \pm 1.5\,\mathrm{Tg\,yr^{-1}}$. These fluxes for cN2O and cF11 match the total long-term troposphere-to-stratosphere flux of N2O and F11, as derived from their stratospheric losses. The cF11 budget is about twice as large as cN2O, because F11 is photolyzed rapidly in the lower–middle stratosphere (~ 24 km) instead of the upper stratosphere like N2O (~ 32 km). The seasonal mean pattern of STE fluxes are shown in Fig. 1. The large majority of STE fluxes enter the troposphere at 25–45° latitude in each hemisphere, but there is a broadening of the northern flux to 65° N in June–July. The importance of this region about the sub-tropical jet for STE is supported by satellite data, where stratospheric folding events (high O_3 in the upper troposphere) are found at the bends of the jet (Tang and Prather, 2010).

Given the small STE fluxes in the core tropics, the Northern Hemisphere (NH) and Southern Hemisphere (SH) fluxes are distinct. The annual mean of NH O_3 STE is $208 \pm 11\,\mathrm{Tg\,yr^{-1}}$ and is slightly larger than the SH mean of $182 \pm 11\,\mathrm{Tg\,yr^{-1}}$. This NH : SH ratio of 53 : 47 is typically found in other studies (Gettelman et al., 1997; Hsu and Prather, 2009; Yang et al., 2016), although some have higher ratios like 58 : 42 (Hegglin and Shepherd, 2009; Meul et al., 2018). In contrast, for cN2O and cF11, the NH flux ($5.1 \pm 0.4\,\mathrm{Tg\,yr^{-1}}$ and $10.6 \pm 0.8\,\mathrm{Tg\,yr^{-1}}$, respectively) is smaller than the SH flux ($6.4 \pm 0.5\,\mathrm{Tg\,yr^{-1}}$ and $12.9 \pm 1.0\,\mathrm{Tg\,yr^{-1}}$, respectively), giving a NH : SH ratio of about 45 : 55. The established view on STE is that the flux is wave driven and under downward control, and thus, the NH flux is much greater than the SH flux (see Table 1 of Holton et al., 1995; also see Appenzeller et al., 1996). Our unexpected results require further analysis, including evidence for hemispheric asymmetry in observations, which is shown in Sect. 4 along with other model metrics.

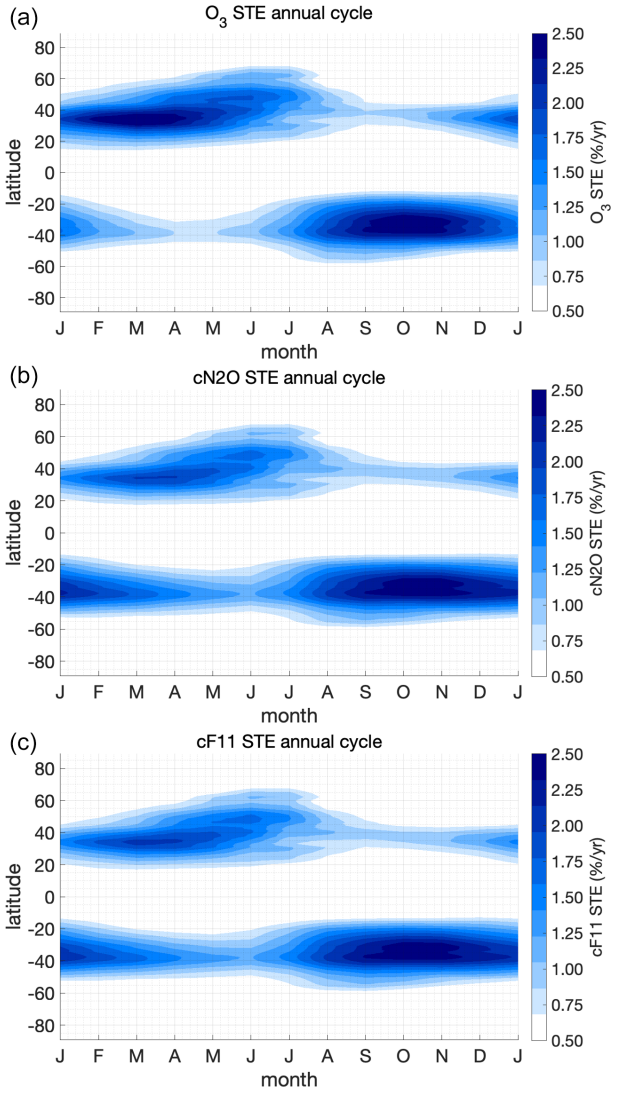

Figure 1. The seasonal (latitude by month) cycle of STE flux (percent per year; hereafter % $\mathrm{yr^{-1}}$) for **(a)** O_3, **(b)** cN2O, and **(c)** cF11. Each month is averaged for years 1990–2017 (e.g., the 28 months of January are averaged). The color bar units are the percent of global and annual mean STE in each bin (1 month by $\sim 1.1°$ latitude).

3.2 Seasonal cycle

The seasonal cycles of STE fluxes summed over global, NH, and SH are shown in Fig. 2. The scales are given as the annual rate (as if the monthly rate were maintained for the year), and each species has a different axis. The right *y* axes are kept at a N2O : F11 ratio of 1 : 2. Despite large differences in the stratospheric chemistry across all three species, the seasonal cycle of STE is highly correlated (Pearson's correlation coef-

Table 1. Summary of key results for the STE flux of O_3 and N_2O presented here (in bold).

	NH	SH	Global	Notes
STE O_3 flux ($TgO_3\,yr^{-1}$)	**208**	**182**	**390**	IFS Cy38r1; years 1990–2017 (this paper; Ruiz et al., 2021)
	239	198	437	IFS Cy36r1; years 2000–2007 (Hsu and Prather, 2014)
	301	233	534	IFS Cy29r1; years 2000–2006 (Hsu and Prather, 2014)
	383	272	655	CMAM; years 1995–2005 (Hegglin and Shepherd, 2009)
STE N_2O flux ($TgN\,yr^{-1}$)	**5.1**	**6.4**	**11.5**	Years 1990–2017, scaled to 320 ppb
			12.9	Using Aura MLS lifetime of 119 years and 320 ppb
LMS $O_3:N_2O$ slope*	**−23.2**	**−17.5**		UCI model
	−19.4	**−15.3**		ACE-FTS observations
	-23 ± 2	-18 ± 3		CMAM model; Fig. 13 of Hegglin and Shepherd (2007)
	-22 ± 4	-14 ± 3		ACE-FTS observations; Hegglin and Shepherd (2007)
			−20.0	Murphy and Fahey (1994)
			−22.0	McLinden et al. (2000)
STE flux $O_3:N_2O$ (mole $mole^{-1}$)	**−23.8**	**−16.6**		UCI model as calculated from entries above
			−29.6	CMAM (Hegglin and Shepherd, 2009), using Aura MLS N_2O lifetime
Best estimate STE O_3 flux ($Tg\,yr^{-1}$)	**60 % to 50 %**	**40 % to 50 %**	$\mathbf{400\pm60}$	Current Antarctic ozone hole conditions; see text

* LMS is the lowermost stratosphere only. For the UCI model, months are selected for highest STE (FMAM or February–May in NH; SOND or September–December in SH; Fig. 1). For the Canadian Middle Atmosphere Model (CMAM), the monthly ranges from their Fig. 13c and d are estimated. Where no reference is given, the source is this paper.

ficient cc > 0.98, except for SH O_3), indicating that all three enter the troposphere from a seasonally near-uniform mixture of $O_3:N2O:F11$ in the lowermost stratosphere.

Global STE peaks in June and reaches a minimum in November. The two hemispheres have dramatically different seasonal amplitudes and somewhat opposite phases. The NH peak STE for all three species occurs in the late boreal spring (May–June), while that in the SH occurs at the start of austral spring (September–October). In the NH, O_3 STE peaks a month before the *c* tracers, and in the SH, the whole annual cycle of O_3 is shifted a month earlier. The NH STE seasonal amplitude is very large for all species ($\sim4:1$ ratio from max to min), with the exchange almost ceasing in the fall. In contrast, the SH STE is more uniform year round, with a $1.5:1$ ratio for cN2O and cF11 and $2.2:1$ for O_3. Other models with similar NH and SH O_3 fluxes show different seasonal amplitudes and phasing (see Fig. 6 in Tang et al., 2021), which will affect tropospheric O_3 abundances. It is important to develop observational metrics that test the seasonality of the lowermost stratosphere related to STE fluxes and to establish monthly STE fluxes as a standard model diagnostic.

An interesting result here is the very tight correlation of the monthly cN2O and cF11 STE, while the O_3 STE is sometimes shifted. Loss of N_2O and F11 occurs at very different altitudes in the tropical stratosphere (~32 and ~24 km, respectively), but both have a similar seasonality in loss, which is driven mostly by the intensity of sunlight along the Earth's orbit (N_2O loss peaks in February and reaches a minimum in July; see Fig. 4 from Prather et al., 2015). Photochemical losses of N_2O and F11 drop quickly for air descending from the altitudes of peak loss in the tropics and, hence, the relative cN2O and cF11 STE fluxes are locked in. O_3, however, continues to evolve photochemically from 24 to 16 km

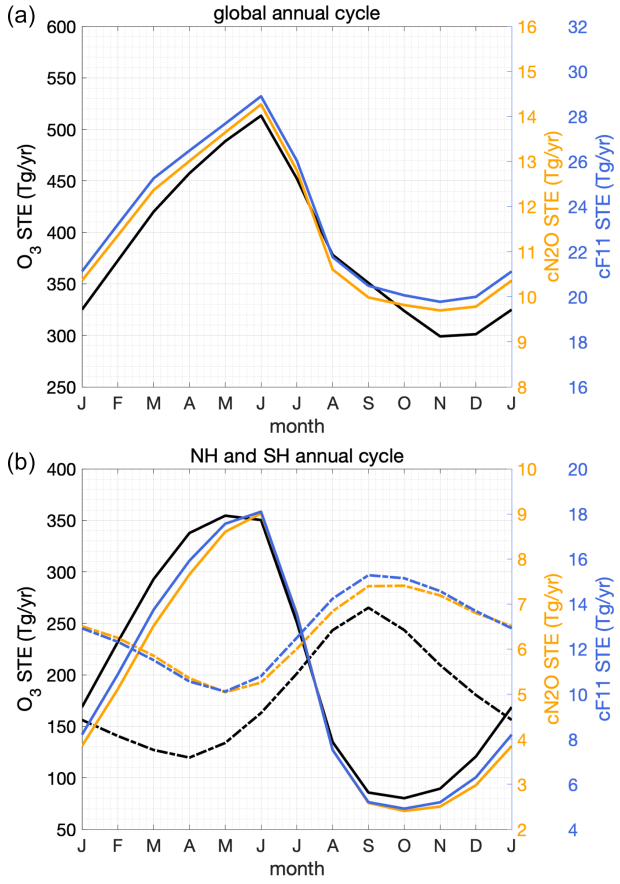

Figure 2. The annual cycle of monthly STE (Tg yr^{-1}) of O_3 (black lines), cN2O (orange lines), and cF11 (blue lines). **(a)** Global STE fluxes and **(b)** hemispheric STE fluxes (NH – solid lines; SH – dashed lines). Each month is averaged for the years 1990–2017 (e.g., the 28 months of January are averaged). Note the different *y* axes for each tracer in each panel.

(upper boundary of the lowermost stratosphere) through net photochemical production in the tropics and loss at mid- and high-latitudes that depends on sunlight and is thus seasonal. There may be observational evidence for the patterns modeled here in the correlation of these three tracers in the lower (16–20 km) and lowermost (12–16 km) extratropical stratosphere (see Sect. 4).

3.3 Interannual variability

Interannual variability (IAV) of N_2O loss and its lifetime is associated primarily with the QBO (most recently, R2021). When the QBO is in its easterly (westerly) phase, the entire overturning circulation is enhanced (suppressed; Baldwin et al., 2001). This results in more (less) air rich in N_2O and F11 being transported from the troposphere to the lower or middle stratosphere, thereby increasing (decreasing) the N_2O and F11 sinks (Prather et al., 2015; Strahan et al., 2015). From the tropical stratosphere, the overturning circulation transports air depleted in N_2O and F11 into the lowermost extratropical stratosphere, where it enters the troposphere. R2021 showed that the observed surface variability in N_2O from this circulation can be modeled and has a clear QBO signal, but it is one that is not strongly correlated with the QBO signal in stratospheric loss.

We generate the IAV of STE fluxes for O_3, cN2O, and cF11 in Fig. 3a, b, and c, with panels for global, NH, and SH. Values are 12-month running means, and so the first modeled point at 1990.5 is the sum of STE for January through December of 1990. In Fig. 3b and c, we also show the seasonal amplitude of STE with double-headed arrows on the left (O_3) and right (cN2O and cF11). In a surprising result, the large NH–SH differences in seasonal amplitude are not reflected in the IAV where NH and SH amplitudes are similar for all three tracers. The QBO modulation of the lowermost stratosphere and STE appears to be unrelated to the seasonal cycle in STE.

Global STE for all three tracers shows QBO-like cycling throughout the 1990–2017 time series. cN2O and cF11 are well correlated (cc ~ 0.9), but either species with O_3 is much less so (cc < 0.7). The hemispheric breakdown provides key information regarding O_3. In the NH, the STE IAV is similar across all three tracers with high correlation coefficients (cc $= 0.82$ for O_3-cN2O, 0.83 for O_3-cF11, and 0.94 for cN2O-cF11). Conversely, in the SH, O_3 STE diverges from the *c* tracer fluxes, showing opposite-sign peaks in 2003 and 2016. The corresponding SH correlations are cc $= 0.38$, 0.65, and 0.85. The loss of the correlation between cN2O and cF11 is unusual because cN2O STE drifts downward relative to cF11 STE, particularly after 2007; nevertheless, the fine structure after 2007 is well matched in both tracers.

In the SH, the massive loss of O_3 within the Antarctic vortex, when mixed with the extra-polar lowermost stratosphere, will systematically shift the O_3 STE to lower values, with less impact on the cN2O and cF11 STE. The IAV of the Antarctic winter vortex, in terms of the amount of O_3 that is depleted (see Fig. 4-4 in WMO, 2018), appears to drive the decorrelation of the SH STE fluxes and is analyzed in Sect. 4.

In the NH, the high variability in the Arctic winter stratosphere can modulate the total O_3 STE flux (e.g., Hsu and Prather, 2009) but appears to maintain the same relative ratio with the cN2O and cF11 fluxes. Model results here indicate that, in the NH, the IAV of O_3, cN2O, and cF11 STE fluxes are synchronized, and thus, the air masses entering the lowermost stratosphere have the same chemical mixtures from year to year. We know that the cold temperature activation of halogen-driven O_3 depletion in the Arctic winter at altitudes above 400 K (potential temperature) can produce large IAV in column ozone (Manney et al., 2011), but the magnitude is still much smaller than in the Antarctic, and it may not reach into the lowermost stratosphere (< 380 K potential temperature). This model accurately simulates Antarctic O_3 loss (Sect. 4), but we have not evaluated it for Arctic loss, and the Arctic conditions operate closer to the thresholds ini-

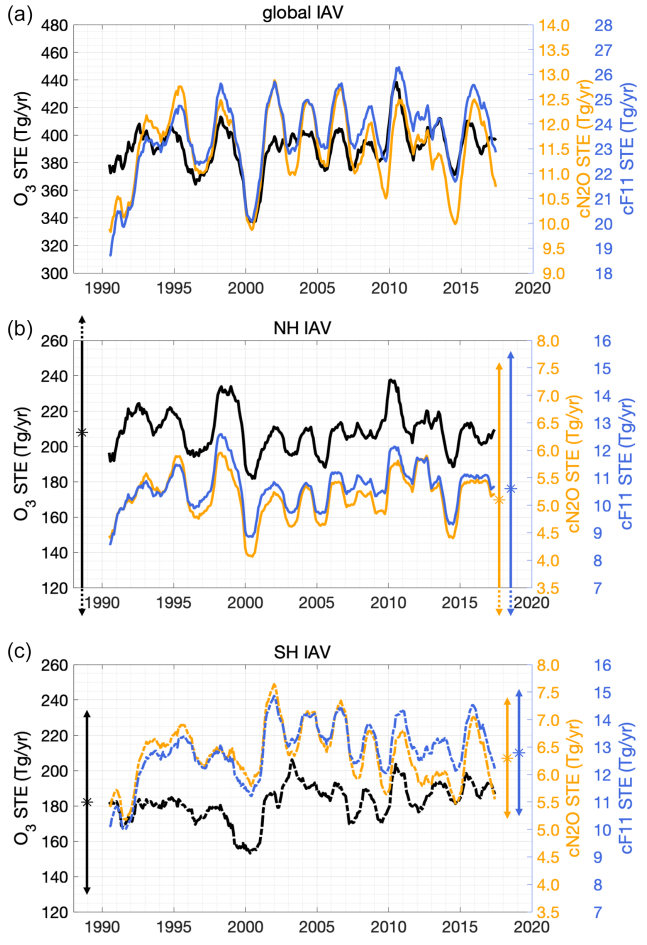

Figure 3. **(a)** Global STE (Tg yr^{-1}), calculated at e90 tropopause, of O_3 (black line; left y axis), cN2O (orange line; orange right y axis), and cF11 (blue line; blue right y axis) for the years 1990–2017. Values are 12-month running means, and so the first point at 1990.5 is the sum of STE for January through December of 1990. **(b)** NH STE. **(c)** SH STE. The scales for cN2O and cF11 are kept in a 1 : 2 ratio. The asterisks and vertical double-headed arrows **(b, c)** depict the seasonal mean and amplitude for each species in each hemisphere.

tiating loss where Linoz v3 chemistry may be inadequate. The same meteorology and transport model with full stratospheric chemistry is able to simulate Arctic O_3 loss (Oslo's CTM2; Isaksen et al., 2012), and thus, it will be possible to re-evaluate the NH IAV with such models or with lowermost stratosphere tracer measurements.

3.4 The link from stratospheric loss to STE flux

What is unusual about the very tight correlation of cN2O and cF11 STE fluxes is that the photochemical loss of N2O and F11 occurs at very different altitudes in the tropical stratosphere, which are not in phase with respect to the QBO, as shown in R2021 (their Fig. 2). The separate phasing of cN2O and cF11 production is lost, presumably by diffusive tracer transport, by the time they reach the extratropical lowermost stratosphere. The overall synchronization of the STE fluxes implies that the absolute STE flux is driven primarily by variations in the venting of the lowermost stratosphere as expected (Holton et al., 1995; Appenzeller et al., 1996) rather than by variations in the chemistry of the middle stratosphere.

This disconnect between the chemical signals generated by the prominent QBO signature of wind reversals, upwelling in the tropical stratosphere, and the STE fluxes is also clear in the magnitude of the loss versus STE. For N_2O, the IAV of cN2O production has a range of $\pm 0.5\,\mathrm{Tg\,yr^{-1}}$, whether from the Aura Microwave Limb Sounder (Aura MLS) observations or the model, whereas the IAV of the cN2O STE flux is $\pm 1.1\,\mathrm{Tg\,yr^{-1}}$. The same is true in relative terms for cF11. Thus, the modulation of the lowermost stratosphere by the QBO is clearly a part of the overall changes in stratospheric circulation related to the QBO (Tung and Yang, 1994a; Kinnersley and Tung, 1999) and is the dominant source of IAV for these three greenhouse gases.

3.5 The QBO signal

To examine the QBO cycle in STE flux, we build a composite pattern (see R2021, Fig. 3, for N_2O surface variations) by synchronizing the STE IAV in Fig. 2 with the QBO cycle. The sync point (offset equal to 0 months) is taken from one of the standard definitions of the QBO phase change, i.e., the shift in sign of the 40 hPa tropical zonal wind from easterly to westerly (Newman, 2020). The 1990–2017 model period has 12 QBO cycles, but we restrict our analysis here to the years 2001–2016 to overlap with the observed surface N_2O data. This period includes seven QBO phase transitions (January 2002, March 2004, April 2006, April 2008, August 2010, April 2013, and July 2015), but the observed surface N_2O is highly anomalous during the QBO centered on August 2010 (R2021), so we remove it from our comparison for consistency with R2021 (see their Fig. S4d). The resulting QBO composites for NH and SH in Fig. 4 span 28 months.

In the NH, the QBO modulation of all three tracers is similar. The STE flux begins to increase at an offset of -8 months and continues to increase slowly for a year, peaking at an offset of $+4$ months; thereafter, it decreases more rapidly in about one-half of a year (offset equal to $+10$). The rise-and-fall cycle takes about 18 months. In the SH, the pattern for cN2O and cF11 is more sinusoidal and is shifted later by ~ 3 months. The SH amplitude of the c tracers is slightly larger relative to the hemispheric mean flux than in the NH, and thus, the SH QBO signal is larger than the NH by about 40 %. Thus, over the typical QBO cycle centered on the sync point, more depleted N_2O and F11 is entering the SH than in the NH. For O_3, the SH modulation of STE is irregular and reduced compared with the NH. Our hypothesis here, consistent with the annual cycle of STE (Fig. 1), is that the

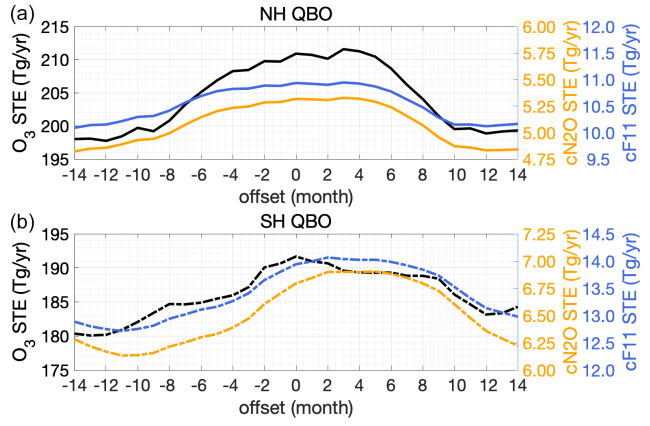

Figure 4. QBO composites of the STE of O_3 (black lines; left y axes), cN2OX (orange lines; orange right y axes), and cF11X (blue lines; blue right y axes) for the **(a)** NH (0–90° N; solid lines) and **(b)** SH (0–90° S; dashed lines). These composites are averages centered on the QBO phase transition at 40 hPa throughout the period of surface observations (years 2001–2016, excluding the August 2010 observed anomaly, for a total of six QBOs). Note that the y axes limits are different for each panel, but the interval scale is consistent for each tracer.

breakup of the Antarctic ozone hole has a major impact on STE, particularly that of O_3, and that its signal has a large IAV that does not synchronize with the QBO. Surprisingly, the large wintertime IAV in the NH Arctic, in the form of sudden stratospheric warmings, does not seem to have a major role in STE fluxes as noted above. This model may miss some of the Arctic O_3 depletion, but it accurately simulates the warmings, which must have a small impact on STE because they do not disrupt the clear QBO signal in the c tracers.

4 Surface variability in N_2O related to STE flux

The surface variability in N_2O is driven by surface emissions, stratospheric loss, and atmospheric transport that mixes the first two signals. R2021 explored the variability originating only from stratospheric chemistry using the decaying tracer N2OX. Here, we use surf-N2O to denote the surface abundances of N2OX when corrected to steady state. R2021 showed that three independent chemistry transport models produced annual and QBO patterns in surface N_2O simply from stratospheric loss. In this paper, we link surf-N2O to the STE cN2O flux, which is linked above to the STE O_3 flux.

The observed surface N_2O, denoted as obs-N_2O and taken from the NOAA network (Dlugokencky et al., 2019), shows a slowly increasing abundance (~ 0.9 ppb yr^{-1}) with a clear signal of annual and interannual variability at some latitudes (see R2021). We calculate the annual and QBO-composite obs-N_2O after detrending and restrict the analysis in this section to the model years 2001–2016 to be consistent with the surface data. The latitude-by-month pattern of obs-N_2O includes the impact of both stratospheric loss (~ 13.5 Tg yr^{-1}) and surface emissions (~ 17 TgN yr^{-1}), with the preponderance of emissions being in the NH (Tian et al., 2020). Total emissions are not expected to have large IAV but may have a seasonal cycle. The seasonal variation in the surface N_2O can also be driven by seasonality in the interhemispheric mixing of the NH–SH gradient (~ 1 ppb).

4.1 Annual cycle

Figure 5 replots the hemispheric mean annual cycles of cN2O STE flux alongside the annual cycles of surf-N2O and obs-N_2O. As noted above, the STE in each hemisphere is almost in opposite phase, as is the modeled surf-N2O (taken from Fig. 5 in R2021). The NH : SH amplitude ratio is about 2.4 : 1 for both STE and surf-N2O. The lag from the peak STE flux of cN2O (negative N_2O) to minimum surf-N2O is about 3 months. Such a 90° phase shift is expected for the seasonal variation in a long-lived tracer relative to a seasonal source or sink. The time lag between the signal at the tropopause and at the surface, the tropospheric turnover time, should be no more than a month. Surprisingly, the cN2O STE seasonal amplitude is much larger in the NH (± 3.4 Tg yr^{-1}) than in the SH (± 1.3 Tg yr^{-1}), although the SH mean (6.5 Tg yr^{-1}) is larger than the NH (5.2 Tg yr^{-1}). Essentially, there is more variability in air depleted in N_2O entering the NH, but air entering the SH has a larger overall deficit. Thus, in our model, the stratosphere creates a NH–SH gradient of $+0.3$ ppb at the surface, which is a significant fraction of the observed the N–S difference of $+1.3$ ppb (R2021). This important result needs to be verified with other models or analyses because it constrains the NH–SH location of sources.

In the NH, as noted in R2021, the two surface abundances, surf-N2O and obs-N_2O, have the same amplitude and phase, implying that, if the model is correct, the emissions-driven surface signal has no seasonality, although we know that some important emissions are seasonal (Butterbach-Bahl et al., 2013). In the SH, the surf-N2O signal is much smaller, in parallel with the small seasonal amplitude in cN2O STE, but it is out of phase with the obs-N_2O. This result implies that the SH has some highly seasonal sources, or simply that the forcing of SH surf-N2O by the seasonal cycle of cN2O is weak. Indeed, this is what we might expect from Fig. 3. In the NH, the seasonal amplitude in N_2O overwhelms the IAV amplitude and is driving the obs-N_2O, but in the SH, both amplitudes are comparable. Given the quasi-regular nature of the QBO, it would interfere with the seasonal cycle and likely change its phase (as found for other models in R2021).

In the NH, the annual cycle of O_3 and cN2O STE are clearly linked. If we accept that the obs-N_2O NH seasonal cycle is simply driven by the STE flux, then how will tropospheric O_3 respond seasonally? A mole fraction scaling of the STE fluxes gives an $O_3 : N_2O$ ratio of ~ 25, and thus,

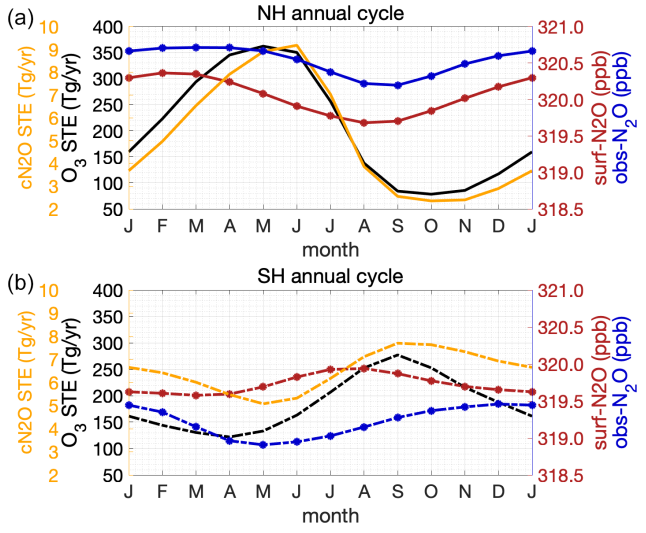

Figure 5. The annual cycle of O_3 and cN2O STE (black and orange lines; left y axes) and the surf-N2O and obs-N_2O (red and blue knotted lines; right y axes) taken from R2021 (see their Fig. 5) for the **(a)** NH and **(b)** SH. cN2O, surf-N2O, and obs-N_2O have been rescaled to reflect that of a tropospheric abundance of 320 ppb. The hemispheric domains for STE are defined as 0–90°, while the surf-N2O and obs-N_2O domain is from 30–90° N/S. Note that the left y axes limits are different between the tracers, but the interval scale is the same.

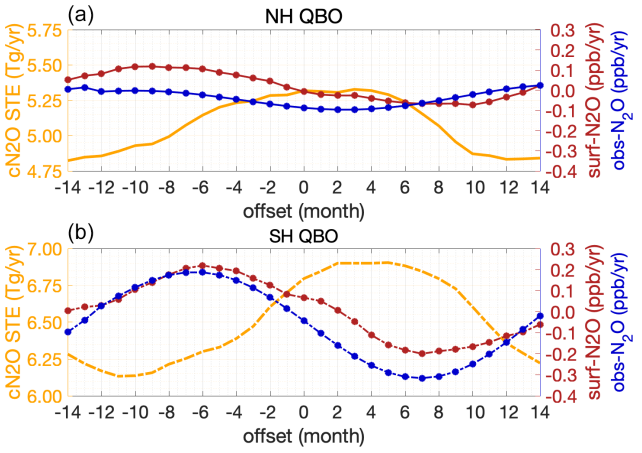

Figure 6. **(a)** NH and **(b)** SH QBO composites of cN2O STE flux (Tg yr^{-1}; orange lines, left axis; Fig. 4) and surf-N2O and obs-N_2O (ppb; red and blue knotted lines, right axes; see Fig. 3 in R2021). Results are shown for the years 2001–2016 (six QBO phase transitions; see Fig. 4). The surf-N2O data are from UCI CTM, and obs-N_2O are taken from NOAA ESRL (Earth System Research Laboratory; see the text).

scaling the surf-N2O amplitude gives a large O_3 surface seasonality of ∼ 18 ppb. However, the residence time of a tropospheric O_3 perturbation is ∼ 1 month, and thus, the peak surface abundance will lag the peak STE flux by only about a month and not by 3 months as for N_2O. O_3 will equilibrate with the flux on monthly timescales and not accumulate. Thus, our estimate is that NH 30–90° surface ozone might increase about 5 ppb, peaking in June, due to the STE flux. In the SH, seasonal patterns are weaker and not well defined, and thus, no obvious STE O_3 signal is expected.

4.2 QBO cycle

The QBO composite of hemispheric mean cN2O STE flux from Fig. 4 is compared with the composite of surface abundances (surf-N2O and obs-N_2O) in Fig. 6. The peak in cN2O flux is broad and flat, but it centers on +2 months for the NH and +4 months for the SH. Unlike the annual cycle, the QBO cycle in STE flux is almost in phase in both hemispheres, with the NH preceding the SH. This phasing of the QBO cycle in surface N_2O was seen with the three models in R2021. In both hemispheres, the modeled surf-N2O peaks before the rise in cN2O and then decreases through most of the period, with elevated cN2O flux as expected. The amplitude of the QBO STE flux is smaller in the NH than SH by about half, and the amplitude of surf-N2O is likewise smaller. The ratio of the amplitudes of surf-N2O to cN2O STE flux is similar in both hemispheres (∼ 0.4 ppb/Tg yr^{-1}), which is encouraging. This ratio is larger than the corresponding one from the annual cycles (∼ 0.1 ppb/Tg yr^{-1}) because the length of the QBO cycle leads to longer accumulation of N_2O-depleted air from the cN2O flux.

In the SH, where the QBO cycle in cN2O flux has a large amplitude, the modeled surf-N2O matches obs-N_2O in amplitude and phase as reported in R2021. In the NH, the comparison of surf-N2O with obs-N_2O is not so good; obs-N2O has a much smaller amplitude and a different phase. This QBO cycle pattern is similar, but reversed, to that of the annual cycle and can be understood in the same way. The NH QBO cycle has a relatively small amplitude, and thus, the interference with the large-amplitude annual cycle adds noise, obscuring the QBO cycle. In the SH it is the opposite, with its weak annual cycle, and the SH QBO cycle is clear. The modeled cN2O fluxes enable us to understand the large-scale variability in the observations.

Thus, for both annual and QBO fluctuations, when the variation in the STE flux is dominated by either cycle, the surface variations are clearly seen and modeled for that cycle. This further supports the findings in R2021, and other studies, that hemispheric surface N_2O variability is driven by stratospheric loss on annual (NH) and QBO (SH) cycles, and it is clearly tied to the STE flux. Given the connection between O_3 and cN2O STE, this relational metric can be used to constrain the O_3 STE for a model ensemble.

5 Lowermost stratosphere

If we accept that matching the observed annual and QBO cycles in surface N_2O constrain the modeled STE cN2O flux,

then how can we use that to also constrain the modeled STE O_3 flux? All evidence, theoretical, observational, and modeled, shows that the STE flux is simultaneous for all species (e.g., Fig. 1) and in proportion to their relative abundances (i.e., tracer : tracer slopes) in the lowermost stratosphere, defined roughly as the region at 100–200 hPa in each hemisphere outside the tropics (Plumb and Ko, 1992).

5.1 The O_3 : N_2O slopes and STE fluxes

We can test the Plumb and Ko (1992) hypothesis in our model framework by comparing the relative STE fluxes for O_3, cN2O, and cF11 with the modeled tracer–tracer slopes in the lowermost stratosphere. These slopes can then be tested using SCISAT-1 ACE-FTS (Scientific Satellite-1 Atmospheric Chemistry Experiment Fourier transform spectrometer) measurements of O_3 and N_2O in the lowermost stratosphere to establish the ratio of the two STE fluxes. The ACE-FTS O_3 : N_2O slopes were used for model transport and chemistry evaluation (Hegglin and Shepherd, 2007) and found to be very sensitive to satellite sampling, except in the lowermost stratosphere.

Figure 7a and b show the N_2O-O_3 slope in each hemisphere taken from the ACE climatology dataset and the UCI CTM. The current ACE dataset (version 3.5) has been curated from measurements made by ACE-FTS from February 2004 to February 2013 (Koo et al., 2017). The SCISAT orbit results in irregular season–latitude coverage, and thus, we average the lowermost stratosphere data over a wide range of latitudes centered on the peak STE flux (20–60° in both hemispheres). For both ACE data and the CTM, we keep to the lowermost stratosphere (200–100 hPa) and average over the 4-month peak of STE flux (February–May in the NH and September–December in the SH; see Fig. 1). Extending into the upper tropical troposphere at 20° helps define the tropospheric endpoint of the slope (low O_3; high N_2O). Our method described here for deriving the slopes from the ACE-FTS data is slightly different from that of Hegglin and Shepherd (2007; e.g., we do not anchor the tropospheric point), and we have the advantage of a longer record.

Based on the long-term mean STE fluxes in the model, we would expect an O_3 : N_2O slope of about −24 (parts per billion of O_3 per part per billion of N_2O; hereafter ppb ppb^{-1}) in the NH and −17 in the SH. The slopes fitted to our modeled grid cell values of O_3 and N2O in the lowermost stratosphere are remarkably similar, with −23.2 (NH) and −17.5 (SH). The ACE data are more scattered but show similar, smaller slopes of −19.4 (NH) and −15.3 (SH). Thus, the NH–SH asymmetry in O_3 versus N_2O STE fluxes is clearly reflected in the tracer–tracer slopes, for both modeled and observed values. Hegglin and Shepherd (2007) had already identified these NH : SH differences when comparing their model to the ACE-FTS observations (their Fig. 13c, d), but implications for STE fluxes were not brought forward.

In the modeled SH (Fig. 7b), one can see strings of points that are samples along neighboring cells and reflect a linear mixing line between two different endpoints, one of which has experienced extensive O_3 depletion (i.e., the Antarctic O_3 hole). We know that there is some chemical loss of O_3 in the NH lowermost polar stratosphere during very cold winters (Manney et al., 2011; Isaksen et al., 2012), but it is not extensive enough to systematically affect the O_3 : N_2O slope over the mid-latitude lowermost stratosphere in either the ACE observations or the CTM simulations.

5.2 IAV of the Antarctic ozone hole and the SH STE O_3 flux

The Antarctic ozone hole appears to be the source of the NH–SH asymmetry in the STE fluxes of O_3 versus N_2O. It is known that the massive chemical depletion of O_3 inside the Antarctic vortex between about 13 and 23 km altitude creates an air mass with lower O_3 : N_2O ratios than usually found in the mid-latitude lowermost stratosphere. When the vortex breaks up, nominally in late November, much of this O_3-depleted air can mix along isentropes into the mid-latitude lowermost stratosphere, changing the O_3 : N_2O ratios and reducing the SH STE O_3 flux.

We have additional information on the SH O_3 STE flux from the year-to-year variations in the size of the ozone hole. The best measure of the scale of Antarctic ozone depletion is the October mean ozone column (DU) averaged from the pole to 63° S equivalent latitude (see Figs. 4–5 in WMO, 2018). When we compare the CTM with the observations (Fig. 8), we find remarkable verisimilitude in the model because the root mean squared difference is 9 DU out of a standard deviation of 29 DU, and the correlation coefficient is 0.96. Thus, we have confidence that we are simulating the correct IAV of the ozone hole. Next, we plot the modeled O_3 STE flux (summed over the 12 months following the peak ozone hole; November–October) with the modeled October ozone column and find a fairly linear relationship. If we estimate the STE O_3 flux before the O_3 hole, when the mean October O_3 column was about 307 DU, then our O_3 flux increases to 209 Tg yr^{-1} (see Fig. 8; red marker), eliminating the hemispheric asymmetry in O_3 STE flux.

The annual deficit in SH STE O_3 flux brought on by the Antarctic ozone hole ranges from about 5 to 55 Tg yr^{-1} and with a central value of 30 Tg yr^{-1} or 14 % of the total. Using the decadal trends 1965–2000 from Hegglin and Shepherd (2009), this deficit is 8 %, and from Meul et al. (2018), it is 5 %. Since both of these models calculate a much larger SH flux ($\sim$ 300 Tg yr^{-1}), we estimate their absolute change in O_3 flux to be 24 and 15 Tg yr^{-1}, respectively. Because the ozone hole effectively removes a fixed, rather than proportional, amount of ozone that presumably is mapped onto the STE flux the following year, we believe the absolute change is the best measure. Thus, the three models estimate the ozone hole causes a deficit in the SH O_3 STE flux in the

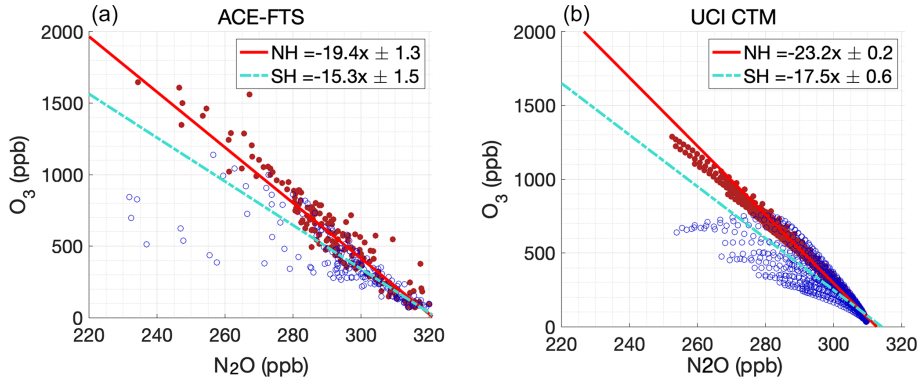

Figure 7. O_3 versus N_2O (x axis) scatterplots from **(a)** SCISAT ACE-FTS and **(b)** the UCI CTM. ACE-FTS data are from monthly climatologies for the period February 2004 to February 2013, restricted to 200–100 hPa, with latitudes of about 20–60° and the months of February–May (NH; red) or September–December (SH; blue). The linear fit lines (ppb ppb^{-1}; values in the legend) are restricted to larger N_2O values (> 280 ppb) to more accurately represent the STE fluxes (see Olsen et al., 2001).

range of 15–30 Tg yr^{-1}. The UCI CTM's ability to match the observed IAV of the ozone hole and to match that linearly with the deficit in STE flux provides support for the upper end of the range. Note that the difference in $O_3 : N_2O$ slopes between NH and SH in Fig. 7 is about 5. If we attribute that solely to the ozone hole and split the flux of N_2O-depleted air evenly between hemispheres, then the ozone-hole-driven O_3 STE flux difference is about 55 Tg yr^{-1}, which is about twice that derived from the variability in our model. This difference in estimated flux indicates that, even without chlorine-driven ozone depletion, the $O_3 : N_2O$ slopes may be inherently different simply because of the strong descent inside the wintertime Antarctic vortex. This can be readily investigated with further model studies.

We looked for any relationship between ozone hole IAV and the STE fluxes of cN2O or cF11 and found mostly a scatterplot with no clear relationship. Given the analysis above, we expect that much of the scatter is related to QBO cycles.

5.3 Other model–measurement metrics related to STE

What else might affect O_3 STE? Stratospheric column O_3 (DU) varies on annual and QBO timescales. These changes in O_3 overhead can have a direct influence on O_3 transport to the troposphere, but the link requires further analysis. Tang et al. (2021) showed the UCI CTM is able to capture the observed annual cycle of stratospheric O_3 column as extracted from total column, using the Ziemke et al. (2019) method. QBO modulation of stratospheric column O_3 has not been fully investigated since Tung and Yang (1994b). Yet, the fluctuations in mass over the annual cycle are comparable to the corresponding variability in O_3 STE flux (1 DU = 10.9 Tg) and likely connected (Fig. 9).

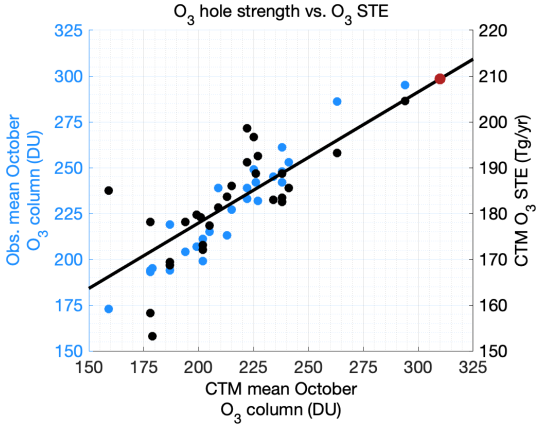

Figure 8. Interannual variability in the observed Antarctic ozone hole from 1990 to 2017 (blue dots; left y axis) versus the CTM-modeled ozone hole (x axis); plus the CTM-modeled SH STE O_3 flux (black dots; right y axis) versus the modeled ozone hole (x axis). The ozone hole is measured by the total ozone column (DU) averaged daily over October, poleward of 63° S in equivalent latitude (see Fig. 4.5 in WMO, 2018). The SH STE O_3 flux (Tg yr^{-1}) is centered on 1 May of the following year (i.e., the 12 months following the nominal breakup of the ozone hole). The black line is a simple regression fit of the modeled STE to the modeled ozone hole (black dots), and the red dot is our estimate of pre-ozone-hole SH STE O_3 flux based on the observed 1979–1982 O_3 column.

6 Conclusions

This work examines how closely O_3 STE is linked to STE fluxes of other trace gases. By including our complementary N_2O and F11 tracers, we can follow the stratospheric loss of these gases along with stratospheric O_3 across the tropopause. The magnitudes of the fluxes are proportional to their abundances in the lower stratosphere, as expected (Plumb and Ko, 1992), and their variability is highly corre-

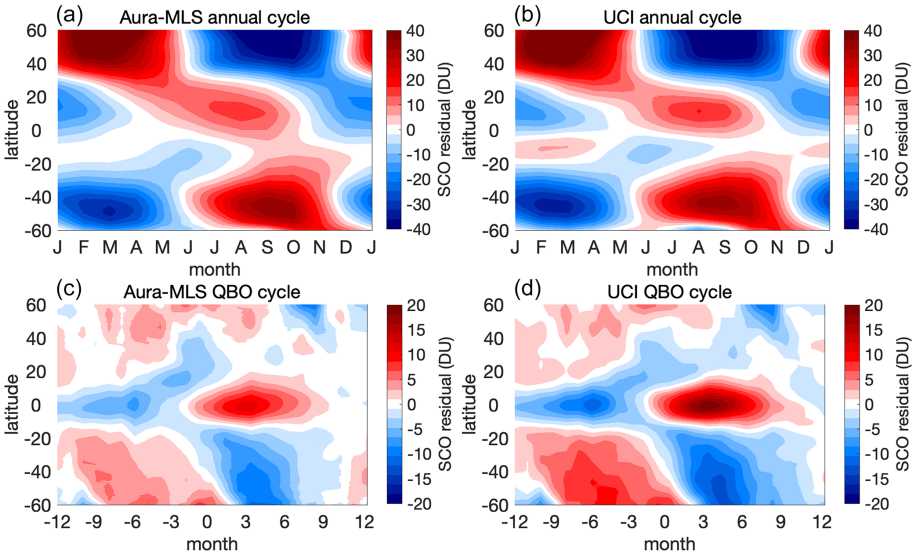

Figure 9. Stratospheric O_3 column residuals taken from Aura MLS **(a, c)** and UCI CTM **(b, d)**, for their mean annual cycle **(a, b)** and mean QBO cycle **(c, d)**, during the years 2005–2017. Residuals are defined at each latitude with a mean of 0 DU.

lated with one another, indicating that they are entering the troposphere simultaneously. Even the distinct QBO pattern of STE fluxes is consistent across O_3, N_2O, and F11. We further constrain the N_2O transport pathway by linking STE of depleted N_2O air with surface fluctuations of N_2O abundance. The surface response in modeled N_2O matches well with the observed surface variability in the SH, indicating that surface variability is driven largely by STE flux.

Consistency of STE O_3 flux. As summarized here, there are a number of model diagnostics and observational constraints that provide a reality check on the consistency of the modeled O_3 STE flux. In Table 1, we examine these for our model and also for the CMAM model (Hegglin and Shepherd, 2007, 2009) because it is one of the few with enough published results. For UCI, we calculate NH : SH fluxes of O_3 ($208 : 182\,\mathrm{Tg\text{-}O_3\,yr^{-1}}$) and N_2O ($5.1 : 6.4\,\mathrm{Tg\text{-}N\,yr^{-1}}$). Thus the mole fraction slopes in the lowermost stratosphere should be -23.8 (NH) and -16.6 (SH). Our model $O_3 : N_2O$ slopes are -23.2 (NH) and -17.5 (SH). Given the seasonal variability and scatter in the correlation plots (Fig. 7), we count this as consistent. For CMAM, the modeled $O_3 : N_2O$ slopes, -23 ± 2 (NH) and -18 ± 3 (SH), are similar to ours and also to the ACE-FTS observations as analyzed by Hegglin and Shepherd (2007), with -22 ± 4 (NH) and -14 ± 3 (SH) or, by us, -19 (NH) and -15 (SH). CMAM does not report the implied STE N_2O fluxes derived from their photochemical loss of N_2O, but their model seems to match observations of N_2O in the middle stratosphere, and so we assume that the Aura-MLS-derived N_2O fluxes are a close estimate ($12.9\,\mathrm{Tg\text{-}N\,yr^{-1}}$). Note that we are using Aura MLS N_2O values here to calculate the photochemical loss, which occurs in the middle to upper stratosphere (see R2021 for the methodology). Just using the CMAM global numbers for O_3 STE flux, we calculate that the $O_3 : N_2O$ slope in the lowermost stratosphere should average to -30. We conclude that their diagnosis of the STE O_3 flux, $655\,\mathrm{Tg\,yr^{-1}}$, is inconsistent with the circulation that generated the $O_3 : N_2O$ slopes and is 50 % too large. We do not view this as a critical assessment of CMAM, since it involves us combining diagnostics from two separate publications and possibly different model simulations, but it is an example of how we might expect future studies of the STE O_3 flux to self-evaluate.

Uncertainty Quantification in STE O_3 flux. Deriving a best estimate and uncertainty from this work involves expert judgment. Changes in meteorological data used by the UCI CTM (IFS cycles 29r1, 36r1, and 38r1, all at 60-layer 1.1° resolution; see Table 1) give a standard deviation in STE of 13 % (only 3 values). If we use observations to derive a value, as in Murphy and Fahey (1994), we must expand our dimensions to the uncertainty in the NH : SH split of N_2O flux to calculate each hemisphere's O_3 flux. The factors are as follows: (1) total STE N_2O flux is $12.9\,\mathrm{Tg\text{-}N\,yr^{-1}}$ from the Aura MLS data, and we assign a ± 10 % 1σ uncertainty; (2) the NH : SH split of the N_2O flux is 44 : 56 in our current model, and was not diagnosed for previous ones, and so we assume a value of 50 : 50 that ranges from 40 : 60 to 60 : 40; (3) analysis of the ACE-FTS observations (ours and Hegglin and Shepherd, 2007) gives $O_3 : N_2O$ slopes of about -21 (NH) and -15 (SH) to which we assign a 1σ uncertainty of ± 3. Propagating these as root mean square errors, we find a ± 15 % uncertainty in the global value, i.e., $400 \pm 60\,\mathrm{Tg\,yr^{-1}}$. Uncertainty in the hemispheric values is more difficult to assess, and from a range of model results shown in Table 1, we can only estimate that the NH : SH ratio is between 60 : 40 and 50 : 50, which is a range that bounds our and CMAM results plus 2 %. Note that this estimate is for current conditions with

Table 2. Metrics from measurements or constrained values for chemistry–climate models (CCMs) related to the stratosphere–troposphere exchange.

Name	Metric	Measured values	Model requirements	Example figure
N_2O loss	Annual and QBO cycles of global mean stratospheric N_2O loss	Monthly N_2O loss calculated from Aura MLS profiles (2005–present)	Stratospheric chemistry for N_2O as tracer; a QBO cycle; monthly mean diagnostics	Fig. 4 (Prather et al., 2015); Fig. 2 (Ruiz et al., 2021); Fig. 3 (this paper)
STE slopes	Matching $O_3 : N_2O$ slopes in lowermost stratosphere	ACE FTS profiles (2004–2013)	Stratospheric O_3 and N_2O calculation (possibly also CFCs); monthly snapshots	Fig. 7 (this paper)
Stratospeheric O_3 column	Annual and QBO composite cycles of stratospheric O_3 column	Monthly zonal mean stratospheric O_3 column from Ziemke et al. (2019) (2005–present)	Stratospheric O_3 chemistry; a QBO cycle; monthly mean diagnostics; separate stratosphere and troposphere O_3 columns	Fig. 9 (this paper)
N_2O loss at surface	Annual and QBO composite cycles of surface N_2O solely from stratospheric loss	NOAA surface N_2O observations	Stratospheric N_2O chemistry; N2OX as a tracer; monthly mean diagnostics	Fig. 3 (Ruiz et al., 2021); Fig. 5 (this paper)
		Constrained (modeled) values		
STE flux of O_3		Monthly, latitude, or hemispheric resolved; net O_3 flux	Run O_3 stratosphere as a tracer; diagnose monthly flux into troposphere, at tropopause or through tropospheric loss of O_3 stratosphere	Figs. 1 and 2 (this paper)
STE flux of N_2O depleted air (also CFC-11)		Monthly, latitude, or hemispheric resolved; STE flux of N_2O (CFC-11)	Run cN2O (cF11) as a tracer; diagnose monthly flux into troposphere	Figs. 1 and 2 (this paper);
SH O_3 hole and flux		Change in SH O_3 STE flux with size of ozone hole; observed IAV of O_3 hole	IAV of ozone hole; daily total O_3 column (lat, long); monthly SH O_3 STE flux	Fig. 7 (this paper)

Note: constrained values are the model-only derived quantities that can be diagnosed from CCMs or CTMs.

a regularly occurring Antarctic ozone hole. We believe the low 50 : 50 ratio is plausible because we have shown that our large SH STE N_2O flux is consistent with the surface QBO variability in N_2O. For years pre-1980, and for when the ozone hole recovers later this century, we anticipate that the SH $O_3 : N_2O$ slope will revert to -18 to -21 and the total STE O_3 flux to 430–460 Tg yr^{-1}. This simplistic estimate is based on a fixed atmospheric circulation.

A major surprise from our model is that the STE flux of O_3 is predominantly NH biased currently and only because of the Antarctic ozone hole. Prior to 1980, and after 2060, it would/will be symmetric between the hemispheres. Our model calculates slightly greater STE fluxes for trace gases like N_2O or F11 in the SH, which is counter to the prevailing theory that the wave-driven fluxes force relatively greater STE in the NH. This difference cannot be directly tested with observations of trace gases, but a range of N_2O hemispheric observations are well modeled and support this premise. More extensive work with multi-model ensembles that include both chemical and dynamical diagnostics in the stratosphere would be needed to overturn the established theory. Our work reemphasizes the importance of trace gas correlations in the lowermost stratosphere as a key observational metric for climate models that may be able to constrain total STE fluxes. The tracer slopes may go beyond just relative STE fluxes because we have other measurements from the upper stratosphere to the surface that constrain, for example, the absolute flux of N_2O better than we first did using just the modeled lifetime.

In Table 2, we gather a set of observation-based model metrics that relate to STE fluxes and will help the community build more robust models to better derive the STE flux of O_3.

Code and data availability. MATLAB code was used to analyze the data and generate the figures and tables in this work. This code, together with the underlying data used in this work, can be accessed through the Dryad repository at https://doi.org/10.7280/D1JX0K (Ruiz, 2021).

Author contributions. DJR and MJP designed and carried out the study and prepared the paper for publication.

Competing interests. The contact author has declared that neither they nor their co-author has any competing interests.

Disclaimer. Publisher's note: Copernicus Publications remains neutral with regard to jurisdictional claims in published maps and institutional affiliations.

Acknowledgements. We thank Xin Zhu, at UCI, for her help in generating the UCI CTM simulations. We gratefully acknowledge the work of the MLS team in producing the level 3 datasets that enabled our MLS-related analyses. Work at the Jet Propulsion Laboratory, California Institute of Technology, was performed under contract with the National Aeronautics and Space Administration. We thank the ACE-FTS team, for making the climatology data used here available for our analyses. The Atmospheric Chemistry Experiment (ACE), also known as SCISAT, is a Canadian-led mission mainly supported by the Canadian Space Agency. We also acknowledge Ed Dlugokencky, for providing the surface N_2O data that were used here to produce an observation-based reference with which to compare our simulated results.

Financial support. The research at UCI has been supported by grants from the National Aeronautics and Space Administration's Modeling, Analysis, and Prediction (MAP) Program (grant no. NNX13AL12G), the Atmospheric Chemistry Modeling and Analysis Program (ACMAP; grant nos. 80NSSC20K1237 and NNX15AE35G), and the National Science Foundation (grant no. NRT-1633631).

Review statement. This paper was edited by Jens-Uwe Grooß and reviewed by two anonymous referees.

References

Appenzeller, C., Holton, J. R., and Rosenlof, K. H.: Seasonal variation of mass transport across the tropopause, J. Geophys. Res.-Atmos., 101, 15071–15078, https://doi.org/10.1029/96JD00821, 1996.

Baldwin, M. P., Gray, L. J., Dunkerton, T. J., Hamilton, K., Haynes, P. H., Randel, W. J., Holton, J. R., Alexander, M. J., Hirota, I., Horinouchi, T., Jones, D. B. A., Kinnersley, J. S., Marquardt, C., Sato, K., and Takahashi, M.: The quasi-biennial oscillation, Rev. Geophys., 39, 179–229, 2001.

Butterbach-Bahl, K., Baggs, E. M., Dannenmann, M., Kiese, R., and Zechmeister-Boltenstern, S.: Nitrous oxide emissions from soils: how well do we understand the processes and their controls?, Philos. T. R. Soc. B, 368, 20130122, https://doi.org/10.1098/rstb.2013.0122, 2013.

Dlugokencky, E. J., Crotwell, A. M., Mund, J. W., Crotwell, M. J., and Thoning, K. W.: Atmospheric Nitrous Oxide Dry Air Mole Fractions from the NOAA ESRL Carbon Cycle Cooperative Global Air Sampling Network, 1997–2018, Version: 2019-07, https://doi.org/10.15138/53g1-x417, 2019.

Gettelman, A., Holton, J. R., and Rosenlof, K. H.: Mass fluxes of O_3, CH_4, N_2O and CF_2Cl_2 in the lower stratosphere calculated from observational data, J. Geophys. Res.-Atmos., 102, 19149–19159, https://doi.org/10.1029/97jd01014, 1997.

Griffiths, P. T., Murray, L. T., Zeng, G., Shin, Y. M., Abraham, N. L., Archibald, A. T., Deushi, M., Emmons, L. K., Galbally, I. E., Hassler, B., Horowitz, L. W., Keeble, J., Liu, J., Moeini, O., Naik, V., O'Connor, F. M., Oshima, N., Tarasick, D., Tilmes, S., Turnock, S. T., Wild, O., Young, P. J., and Zanis, P.: Tropospheric ozone in CMIP6 simulations, Atmos. Chem. Phys., 21, 4187–4218, https://doi.org/10.5194/acp-21-4187-2021, 2021.

Hamilton, K. and Fan, S. M.: Effects of the stratospheric quasi-biennial oscillation on long-lived greenhouse gases in the troposphere, J. Geophys. Res.-Atmos., 105, 20581–20587, https://doi.org/10.1029/2000jd900331, 2000.

Hegglin, M. I. and Shepherd, T. G.: O_3-N_2O correlations from the Atmospheric Chemistry Experiment: Revisiting a diagnostic of transport and chemistry in the stratosphere, J. Geophys. Res.-Atmos., 112, D19301, https://doi.org/10.1029/2006jd008281, 2007.

Hegglin, M. I. and Shepherd, T. G.: Large climate-induced changes in ultraviolet index and stratosphere-to-troposphere ozone flux, Nat. Geosci., 2, 687–691, https://doi.org/10.1038/Ngeo604, 2009.

Hess, P., Kinnison, D., and Tang, Q.: Ensemble simulations of the role of the stratosphere in the attribution of northern extratropical tropospheric ozone variability, Atmos. Chem. Phys., 15, 2341–2365, https://doi.org/10.5194/acp-15-2341-2015, 2015.

Hirsch, A. I., Michalak, A. M., Bruhwiler, L. M., Peters, W., Dlugokencky, E. J., and Tans, P. P.: Inverse modeling estimates of the global nitrous oxide surface flux from 1998–2001, Global Biogeochem. Cy., 20, Gb1008, https://doi.org/10.1029/2004gb002443, 2006.

Holton, J. R.: On the Global Exchange of Mass between the Stratosphere and Troposphere, J. Atmos. Sci., 47, 392–395, https://doi.org/10.1175/1520-0469(1990)047<0392:Otgeom>2.0.Co;2, 1990.

Holton, J. R., Haynes, P. H., Mcintyre, M. E., Douglass, A. R., Rood, R. B., and Pfister, L.: Stratosphere-Troposphere Exchange, Rev. Geophys., 33, 403–439, 1995.

Hsu, J. and Prather, M. J.: Stratospheric variability and tropospheric ozone, J. Geophys. Res.-Atmos., 114, D06102, https://doi.org/10.1029/2008jd010942, 2009.

Hsu, J. and Prather, M. J.: Global long-lived chemical modes excited in a 3-D chemistry transport model: Stratospheric N_2O, NO_y, O_3 and CH_4 chemistry, Geophys. Res. Lett., 37, L07805, L07805, https://doi.org/10.1029/2009gl042243, 2010.

Hsu, J. N. and Prather, M. J.: Is the residual vertical velocity a good proxy for stratosphere-troposphere exchange of ozone?, Geophys. Res. Lett., 41, 9024–9032, https://doi.org/10.1002/2014GL061994, 2014.

Hsu, J., Prather, M. J., and Wild, O.: Diagnosing the stratosphere-to-troposphere flux of ozone in a chemistry transport model, J. Geophys. Res.-Atmos., 110, D19305, https://doi.org/10.1029/2005jd006045, 2005.

Isaksen, I. S. A., Zerefos, C., Wang, W. C., Balis, D., Eleftheratos, K., Rognerud, B., Stordal, F., Berntsen, T. K., LaCasce, J. H., Sovde, O. A., Olivie, D., Orsolini, Y. J., Zyrichidou, I., Prather, M., and Tuinder, O. N. E.: Attribution of the Arctic ozone column deficit in March 2011, Geophys. Res. Lett., 39, L24810, https://doi.org/10.1029/2012gl053876, 2012.

Kinnersley, J. S. and Tung, K. K.: Mechanisms for the extratropical QBO in circulation and ozone, J Atmos Sci, 56, 1942–1962, https://doi.org/10.1175/1520-0469(1999)056<1942:Mfteqi>2.0.Co;2, 1999.

Koo, J. H., Walker, K. A., Jones, A., Sheese, P. E., Boone, C. D., Bernath, P. F., and Manney, G. L.: Global climatology based on the ACE-FTS version 3.5 dataset: Addition of mesospheric levels and carbon-containing species in the UTLS, J. Quant. Spectrosc. Ra., 186, 52–62, https://doi.org/10.1016/j.jqsrt.2016.07.003, 2017.

Liang, Y. X., Gillett, N. P., and Monahan, A. H.: Climate Model Projections of 21st Century Global Warming Constrained Using the Observed Warming Trend, Geophys. Res. Lett., 47, e2019GL086757, https://doi.org/10.1029/2019GL086757, 2020.

Liu, H., Considine, D. B., Horowitz, L. W., Crawford, J. H., Rodriguez, J. M., Strahan, S. E., Damon, M. R., Steenrod, S. D., Xu, X., Kouatchou, J., Carouge, C., and Yantosca, R. M.: Using beryllium-7 to assess cross-tropopause transport in global models, Atmos. Chem. Phys., 16, 4641–4659, https://doi.org/10.5194/acp-16-4641-2016, 2016.

Manney, G. L., Santee, M. L., Rex, M., Livesey, N. J., Pitts, M. C., Veefkind, P., Nash, E. R., Wohltmann, I., Lehmann, R., Froidevaux, L., Poole, L. R., Schoeberl, M. R., Haffner, D. P., Davies, J., Dorokhov, V., Gernandt, H., Johnson, B., Kivi, R., Kyro, E., Larsen, N., Levelt, P. F., Makshtas, A., McElroy, C. T., Nakajima, H., Parrondo, M. C., Tarasick, D. W., von der Gathen, P., Walker, K. A., and Zinoviev, N. S.: Unprecedented Arctic ozone loss in 2011, Nature, 478, 469–475, https://doi.org/10.1038/nature10556, 2011.

McLinden, C. A., Olsen, S. C., Hannegan, B., Wild, O., Prather, M. J., and Sundet, J.: Stratospheric ozone in 3-D models: A simple chemistry and the cross-tropopause flux, J. Geophys. Res.-Atmos., 105, 14653–14665, https://doi.org/10.1029/2000JD900124, 2000.

Meul, S., Langematz, U., Kröger, P., Oberländer-Hayn, S., and Jöckel, P.: Future changes in the stratosphere-to-troposphere ozone mass flux and the contribution from climate change and ozone recovery, Atmos. Chem. Phys., 18, 7721–7738, https://doi.org/10.5194/acp-18-7721-2018, 2018.

Montzka, S. A., Dutton, G. S., Yu, P. F., Ray, E., Portmann, R. W., Daniel, J. S., Kuijpers, L., Hall, B. D., Mondeel, D., Siso, C., Nance, D., Rigby, M., Manning, A. J., Hu, L., Moore, F., Miller, B. R., and Elkins, J. W.: An unexpected and persistent increase in global emissions of ozone-depleting CFC-11, Nature, 557, 413–416, https://doi.org/10.1038/s41586-018-0106-2, 2018.

Murphy, D. M. and Fahey, D. W.: An estimate of the flux of stratospheric reactive nitrogen and ozone into the troposphere, J. Geophys. Res., 99, 5325–5332, 1994.

Nevison, C. D., Kinnison, D. E., and Weiss, R. F.: Stratospheric influences on the tropospheric seasonal cycles of nitrous oxide and chlorofluorocarbons, Geophys. Res. Lett., 31, L20103, https://doi.org/10.1029/2004gl020398, 2004.

Nevison, C. D., Mahowald, N. M., Weiss, R. F., and Prinn, R. G.: Interannual and seasonal variability in atmospheric N_2O, Global Biogeochem. Cy., 21, Gb3017, https://doi.org/10.1029/2006gb002755, 2007.

Newman, P.: The quasi-biennial oscillation (QBO), NASA, Goddard Space Flight Center, available at: https://acd-ext.gsfc.nasa.gov/Data_services/met/qbo/qbo.html, last access: 3 March 2020.

Olsen, M. A., Schoeberl, M. R., and Douglass, A. R.: Stratosphere-troposphere exchange of mass and ozone, J. Geophys. Res.-Atmos., 109, D24114, https://doi.org/10.1029/2004jd005186, 2004.

Olsen, M. A., Manney, G. L., and Liu, J. H.: The ENSO and QBO Impact on Ozone Variability and Stratosphere-Troposphere Exchange Relative to the Subtropical Jets, J. Geophys. Res.-Atmos., 124, 7379–7392, https://doi.org/10.1029/2019JD030435, 2019.

Olsen, S. C., McLinden, C. A., and Prather, M. J.: Stratospheric N_2O-NO_y system: testing uncertainties in a three-dimensional framework, J. Geophys. Res., 106, 28771–28784, 2001.

Plumb, R. A. and Ko, M. K. W.: Interrelationships between Mixing Ratios of Long Lived Stratospheric Constituents, J. Geophys. Res.-Atmos., 97, 10145–10156, 1992.

Prather, M. J., Zhu, X., Tang, Q., Hsu, J., and Neu, J. L.: An atmospheric chemist in search of the tropopause, J. Geophys. Res., 116, D04306, https://doi.org/10.1029/2010jd014939, 2011.

Prather, M. J., Hsu, J., DeLuca, N. M., Jackman, C. H., Oman, L. D., Douglass, A. R., Fleming, E. L., Strahan, S. E., Steenrod, S. D., Sovde, O. A., Isaksen, I. S. A., Froidevaux, L., and Funke, B.: Measuring and modeling the lifetime of nitrous oxide including its variability, J. Geophys. Res.-Atmos., 120, 5693–5705, https://doi.org/10.1002/2015JD023267, 2015.

Ray, E. A., Portmann, R. W., Yu, P. F., Daniel, J., Montzka, S. A., Dutton, G. S., Hall, B. D., Moore, F. L., and Rosenlof, K. H.: The influence of the stratospheric Quasi-Biennial Oscillation on trace gas levels at the Earth's surface, Nat. Geosci., 13, 22–24, https://doi.org/10.1038/s41561-019-0507-3, 2020.

Ruiz, D.: Data and code from: How atmospheric chemistry and transport drive surface variability of N2O and CFC-11, Dryad [data set], https://doi.org/10.7280/D1JX0K, 2021.

Ruiz, D. J., Prather, M. J., Strahan, S. E., Thompson, R. L., Froidevaux, L., and Steenrod, S. D.: How Atmospheric Chemistry and Transport Drive Surface Variability of N_2O and CFC-11, J. Geophys. Res.-Atmos., 126, e2020JD033979, https://doi.org/10.1029/2020JD033979, 2021.

Stohl, A., Bonasoni, P., Cristofanelli, P., Collins, W., Feichter, J., Frank, A., Forster, C., Gerasopoulos, E., Gaggeler, H., James, P., Kentarchos, T., Kromp-Kolb, H., Kruger, B., Land, C., Meloen, J., Papayannis, A., Priller, A., Seibert, P., Sprenger, M., Roelofs, G. J., Scheel, H. E., Schnabel, C., Siegmund, P., Tobler, L., Trickl, T., Wernli, H., Wirth, V., Zanis, P., and Zerefos, C.: Stratosphere-troposphere exchange: A review, and what we have learned from STACCATO, J. Geophys. Res.-Atmos., 108, 8516, https://doi.org/10.1029/2002jd002490, 2003.

Strahan, S. E., Douglass, A. R., Stolarski, R. S., Akiyoshi, H., Bekki, S., Braesicke, P., Butchart, N., Chipperfield, M. P., Cugnet, D., Dhomse, S., Frith, S. M., Gettelman, A., Hardiman, S. C., Kinnison, D. E., Lamarque, J. F., Mancini, E., Marchand, M., Michou, M., Morgenstern, O., Nakamura, T., Olivie, D., Pawson, S., Pitari, G., Plummer, D. A., Pyle, J. A., Scinocca, J. F., Shepherd, T. G., Shibata, K., Smale, D., Teyssedre, H., Tian,

W., and Yamashita, Y.: Using transport diagnostics to understand chemistry climate model ozone simulations, J. Geophys. Res.-Atmos., 116, D17302, https://doi.org/10.1029/2010jd015360, 2011.

Strahan, S. E., Oman, L. D., Douglass, A. R., and Coy, L.: Modulation of Antarctic vortex composition by the quasi-biennial oscillation, Geophys. Res. Lett., 42, 4216–4223, https://doi.org/10.1002/2015GL063759, 2015.

Tang, Q. and Prather, M. J.: Correlating tropospheric column ozone with tropopause folds: the Aura-OMI satellite data, Atmos. Chem. Phys., 10, 9681–9688, https://doi.org/10.5194/acp-10-9681-2010, 2010.

Tang, Q., Hess, P. G., Brown-Steiner, B., and Kinnison, D. E.: Tropospheric ozone decrease due to the Mount Pinatubo eruption: Reduced stratospheric influx, Geophys. Res. Lett., 40, 5553–5558, https://doi.org/10.1002/2013GL056563, 2013.

Tang, Q., Prather, M. J., Hsu, J., Ruiz, D. J., Cameron-Smith, P. J., Xie, S., and Golaz, J.-C.: Evaluation of the interactive stratospheric ozone (O3v2) module in the E3SM version 1 Earth system model, Geosci. Model Dev., 14, 1219–1236, https://doi.org/10.5194/gmd-14-1219-2021, 2021.

Thompson, R. L., Patra, P. K., Ishijima, K., Saikawa, E., Corazza, M., Karstens, U., Wilson, C., Bergamaschi, P., Dlugokencky, E., Sweeney, C., Prinn, R. G., Weiss, R. F., O'Doherty, S., Fraser, P. J., Steele, L. P., Krummel, P. B., Saunois, M., Chipperfield, M., and Bousquet, P.: TransCom N_2O model inter-comparison – Part 1: Assessing the influence of transport and surface fluxes on tropospheric N_2O variability, Atmos. Chem. Phys., 14, 4349–4368, https://doi.org/10.5194/acp-14-4349-2014, 2014.

Tian, H. Q., Xu, R. T., Canadell, J. G., Thompson, R. L., Winiwarter, W., Suntharalingam, P., Davidson, E. A., Ciais, P., Jackson, R. B., Janssens-Maenhout, G., Prather, M. J., Regnier, P., Pan, N. Q., Pan, S. F., Peters, G. P., Shi, H., Tubiello, F. N., Zaehle, S., Zhou, F., Arneth, A., Battaglia, G., Berthet, S., Bopp, L., Bouwman, A. F., Buitenhuis, E. T., Chang, J. F., Chipperfield, M. P., Dangal, S. R. S., Dlugokencky, E., Elkins, J. W., Eyre, B. D., Fu, B. J., Hall, B., Ito, A., Joos, F., Krummel, P. B., Landolfi, A., Laruelle, G. G., Lauerwald, R., Li, W., Lienert, S., Maavara, T., MacLeod, M., Millet, D. B., Olin, S., Patra, P. K., Prinn, R. G., Raymond, P. A., Ruiz, D. J., van der Werf, G. R., Vuichard, N., Wang, J. J., Weiss, R. F., Wells, K. C., Wilson, C., Yang, J., and Yao, Y. Z.: A comprehensive quantification of global nitrous oxide sources and sinks, Nature, 586, 248–252, https://doi.org/10.1038/s41586-020-2780-0, 2020.

Tokarska, K. B., Stolpe, M. B., Sippel, S., Fischer, E. M., Smith, C. J., Lehner, F., and Knutti, R.: Past warming trend constrains future warming in CMIP6 models, Sci. Adv., 6, eaaz9549, https://doi.org/10.1126/sciadv.aaz9549, 2020.

Tung, K. K. and Yang, H.: Global QBO in Circulation and Ozone 2. A Simple Mechanistic Model, J. Atmos. Sci., 51, 2708–2721, https://doi.org/10.1175/1520-0469(1994)051<2708:Gqicao>2.0.Co;2, 1994a.

Tung, K. K. and Yang, H.: Global QBO in Circulation and Ozone 1. Reexamination of Observational Evidence, J. Atmos. Sci., 51, 2699–2707, https://doi.org/10.1175/1520-0469(1994)051<2699:Gqicao>2.0.Co;2, 1994b.

Williams, R. S., Hegglin, M. I., Kerridge, B. J., Jöckel, P., Latter, B. G., and Plummer, D. A.: Characterising the seasonal and geographical variability in tropospheric ozone, stratospheric influence and recent changes, Atmos. Chem. Phys., 19, 3589–3620, https://doi.org/10.5194/acp-19-3589-2019, 2019.

WMO: Scientific Assessment of Ozone Depletion: 2018, Global Ozone Research and Monitoring Project – Report No. 58, World Meteorological Organization, Geneva, Switzerland, 588 pp., available at: https://csl.noaa.gov/assessments/ozone/2018/ (last access: January 2021), 2018.

Yang, H., Chen, G., Tang, Q., and Hess, P.: Quantifying isentropic stratosphere-troposphere exchange of ozone, J. Geophys. Res.-Atmos., 121, 3372–3387, https://doi.org/10.1002/2015JD024180, 2016.

Young, P. J., Archibald, A. T., Bowman, K. W., Lamarque, J.-F., Naik, V., Stevenson, D. S., Tilmes, S., Voulgarakis, A., Wild, O., Bergmann, D., Cameron-Smith, P., Cionni, I., Collins, W. J., Dalsøren, S. B., Doherty, R. M., Eyring, V., Faluvegi, G., Horowitz, L. W., Josse, B., Lee, Y. H., MacKenzie, I. A., Nagashima, T., Plummer, D. A., Righi, M., Rumbold, S. T., Skeie, R. B., Shindell, D. T., Strode, S. A., Sudo, K., Szopa, S., and Zeng, G.: Preindustrial to end 21st century projections of tropospheric ozone from the Atmospheric Chemistry and Climate Model Intercomparison Project (ACCMIP), Atmos. Chem. Phys., 13, 2063–2090, https://doi.org/10.5194/acp-13-2063-2013, 2013.

Young, P. J., Naik, V., Fiore, A. M., Gaudel, A., Guo, J., Lin, M. Y., Neu, J. L., Parrish, D. D., Rieder, H. E., Schnell, J. L., Tilmes, S., Wild, O., Zhang, L., Ziemke, J., Brandt, J., Delcloo, A., Doherty, R. M., Geels, C., Hegglin, M. I., Hu, L., Im, U., Kumar, R., Luhar, A., Murray, L., Plummer, D., Rodriguez, J., Saiz-Lopez, A., Schultz, M. G., Woodhouse, M. T., and Zeng, G.: Tropospheric Ozone Assessment Report: Assessment of global-scale model performance for global and regional ozone distributions, variability, and trends, Elementa-Science of the Anthropocene, 6, 10, https://doi.org/10.1525/elementa.265, 2018.

Zeng, G., Morgenstern, O., Braesicke, P., and Pyle, J. A.: Impact of stratospheric ozone recovery on tropospheric ozone and its budget, Geophys. Res. Lett., 37, L09805, https://doi.org/10.1029/2010gl042812, 2010.

Ziemke, J. R., Oman, L. D., Strode, S. A., Douglass, A. R., Olsen, M. A., McPeters, R. D., Bhartia, P. K., Froidevaux, L., Labow, G. J., Witte, J. C., Thompson, A. M., Haffner, D. P., Kramarova, N. A., Frith, S. M., Huang, L.-K., Jaross, G. R., Seftor, C. J., Deland, M. T., and Taylor, S. L.: Trends in global tropospheric ozone inferred from a composite record of TOMS/OMI/MLS/OMPS satellite measurements and the MERRA-2 GMI simulation, Atmos. Chem. Phys., 19, 3257–3269, https://doi.org/10.5194/acp-19-3257-2019, 2019.